Three-Dimensional Flow Transport Modes in Directional Solidification During Space Processing

W. A. Arnold,* D. A. Jacqmin,† R. L. Gaug,‡ and A. Chait§
NASA Lewis Research Center, Cleveland, Ohio 44135

A numerical model for the proposed GTE GaAs space experiment is presented. The model includes the actual ampule design and the experimentally obtained furnace thermal profiles. It is demonstrated that the commonly presumed axisymmetric flows in numerical studies are physically reasonable only when the local gravitational acceleration vector is parallel to the ampule's axis. Other gravitational orientations result in nontrivial three-dimensional flows that must be resolved using full three-dimensional models. Implications of the resulting flow and thermal fields on the growing crystal at conditions available during space processing are also discussed.

Nomenclature

C_p = specific heat
g = gravity
k = thermal conductivity
p = pressure
T = temperature
t = time
u, v, w = velocity
β = thermal expansion coefficient
μ = viscosity
ρ = density

Introduction

THE directional solidification process is an excellent case of the manner in which modeling can result in a better understanding of transport phenomena in material processes, ultimately leading to improved crystal quality. During the past decade, great strides have been taken in the design of efficient algorithms and models, which include most of the important features of such experiments (see, for example, the review article by Brown[1]).

The phenomena involved in solidification from the melt are rather complex. Several time and length scales spanning many orders of magnitude are simultaneously responsible for setting the flow, thermal, and solutal fields. Other complicating effects to be considered are time dependency, multidimensionality, flow transitions, and the presence of unspecified solidification front(s). In light of these difficulties, it is not surprising that several important and unique aspects of space processing are presently not addressed, even in the more sophisticated models. In particular, the residual gravitational acceleration vector, while nominally several orders of magnitudes smaller than 1 gau (gravitational acceleration unit, or 9.81 m/s^2), is generally time-dependent, and has components along all three principal axes. Even ignoring the time dependency of the problem (see Alexander et al.[2]), one is still left with the inherent three-dimensionality of the driving force.

Presented as Paper 90-0409 at the AIAA 28th Aerospace Sciences Meeting, Reno, NV, Jan. 8-11, 1990; received Feb. 11, 1990; revision received June 8, 1990; accepted for publication June 21, 1990.

*Resident Research Associate, MS 105-1. Student Member AIAA.
†Research Scientist, MS 5-11.
‡Resident Research Associate, MS 105-1.
§Research Scientist, MS 105-1.

Most directional solidification experiments utilize some variant of the classical Bridgman-Stockbarger apparatus. The aspect ratio of the ampule is usually sufficiently large so that quasi-steady-state solidification conditions are reached. Most analyses to date exploit this feature in the problem formulation stage. However, this assumption is often unacceptable for short aspect-ratio ampules, in which the heat transfer (and consequently the flowfield) is dependent upon the boundary conditions at the ampule's longitudinal ends. Such a solidification process never reaches a steady-state condition, and necessitates a fully transient simulation that includes the thermal end effects.

Another essential but relatively unaccounted for ingredient in the current state of knowledge is the question of the means by which the transport processes are altered by the three-dimensionality of the driving mechanism. One cannot assume that the simplification of an axisymmetric model is justified a priori, because this condition can be valid only for a gravity vector orientation parallel to the ampule's longitudinal axis. Several flow regimes driven by both thermal gradients in the system (longitudinally as well as radially) are possible. Some are indeed axisymmetric, but most are three-dimensional in nature.

The purpose of this study is to examine several flow regimes that may arise in typical space processing. These regimes are computed for an actual experiment, i.e., the GTE GaAs space experiment (Kafalas et al.[3]), expected to fly on STS in May 1991. This experiment involves the directional solidification, in a gradient freeze furnace, of a relatively large diameter boule of GaAs with a short aspect ratio. Both end effects and time-dependent aspects of the problem must be considered in a complete simulation of the experiment. The analysis presented here is restricted to the examination of three-dimensional effects due to gravity vector orientation. Although the model includes all the important geometrical features of the ampule, including end effects, the implications of the time-dependent solidification on the experiment will be discussed elsewhere.

Experimental Apparatus

The details of the furnace and ampule design are shown in Figs. 1 and 2. Briefly, the experiment will be flown as a get-away-special package, which includes two separate furnaces. Each of the 6-in. diameter and 12-in. long furnaces use a multizone coil heater. A novel ampule design eliminates possible free surfaces in the melt resulting from solidification shrinkage by using a pyrolytic boron nitride (PBN) spring and a movable graphite piston. In the gradient freeze mode, the power is reduced to accommodate about 5-6 μm/s growth rate, resulting in a complete solidification of the 1-in. diameter by 4-in. long GaAs boule in about 4 h. Selenium is used as a

dopant material for assessing the effects of gravity-driven convection on the segregation fields, and interface demarcation is obtained by Peltier pulsing. The furnace thermal environment is measured by five thermocouples placed outside the ampule, such that reasonable spatial and temporal thermal boundary conditions are available for the simulations. The gap between the ampule and the furnace is sufficiently small so that the shape factor between points on the ampule and points on the furnace (at the same axial position) is essentially united. Therefore, it was not necessary to include view factors in these calculations. The data from one ground test are used in this study.

Governing Equations and Numerical Methods

The governing equations [Eqs. (1-3)] are the incompressible Navier-Stokes equations written in a three-dimensional Cartesian system. The r-x axisymmetric version of the equations was used for the restricted two-dimensional simulations. The Oberback-Boussinesq approximation for density variations is used, which is justified in this case because of the relatively low thermal gradients present in the melt

$$u_{i,i} = 0 \tag{1}$$

$$\rho[\partial u_i/\partial t + u_j u_{i,j}] = -p_i + \rho f_i + \rho g_i[1 - \beta(T - T_B)] + [\mu(u_{i,j} + u_{j,i}]_j \tag{2}$$

$$\rho C_p[\partial T/\partial t + u_j T_j] = (kT_j)_j \tag{3}$$

The set of equations is solved using a modified version of FIDAP, a finite element based code.[4] Nonslip boundary conditions are imposed on all solid walls. The thermal environment as established by the furnace is applied to the ampule via nonlinearized radiation heat transfer, in which the furnace temperature is allowed to vary in both position and time along the ampule, as dictated by the experimental data. Due to the complicated construction and the short aspect ratio of the ampule, the commonly used pseudo-steady-state model[5] is inadequate for this case. In particular, both end effects and time-dependent solidification conditions are critical for this experiment and must be included in the model.

The ampule configuration, as modeled in this study, is shown in Fig. 3a. The thermal boundary conditions mentioned earlier were imposed on the PBN outer layer, and internal solid conduction in the various materials comprising the ampule was treated as a conjugated problem in the simulations. The entire GaAs boule was modeled as fluid whose transport properties were varied sharply through a small finite zone around the melting temperature. In this approach solid portions of the GaAs were immobilized by designating an extremely high viscosity to portions below the melting temperature. Thus, the interface shape can be located by tracking the melting temperature isotherm. The heat of fusion was introduced via one of several enthalpy algorithms.[6,7] This fixed-grid approach is fast and sufficiently accurate for this case. The interface was usually resolved to within 0.1°C.

The results were checked for convergence to within a specified tolerance (0.001) of both the normalized velocity and the

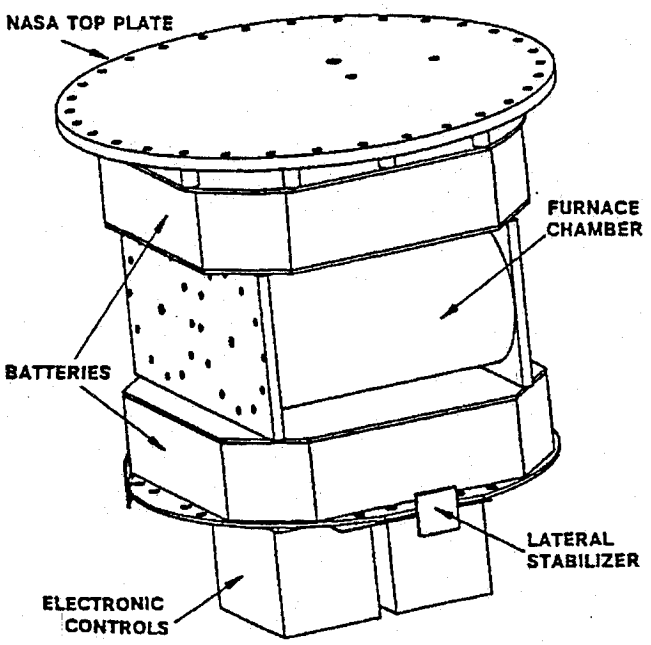

Fig. 1 GTE GaAs get-away-special payload.

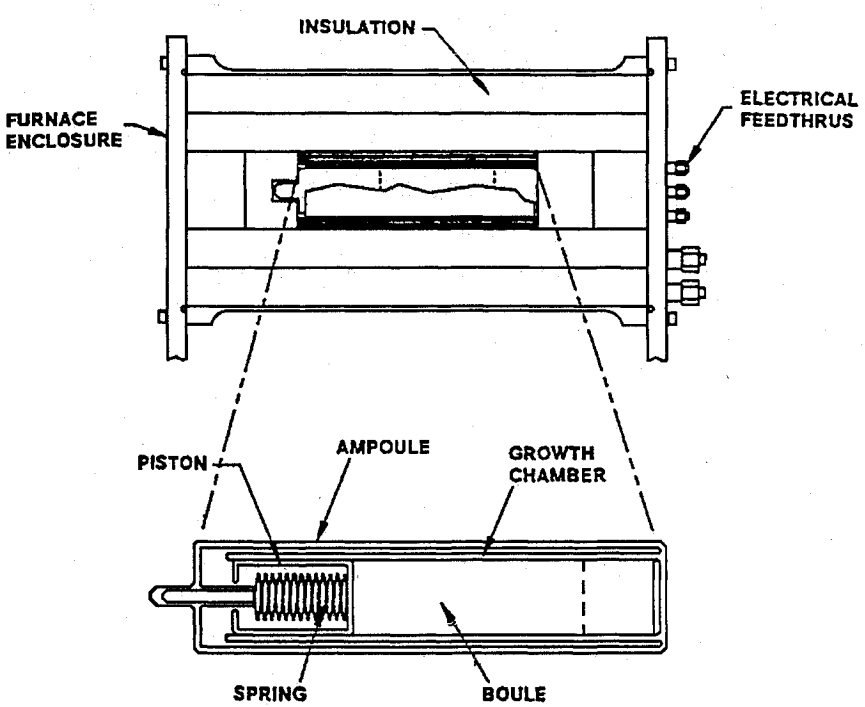

Fig. 2 Furnace and ampule details.

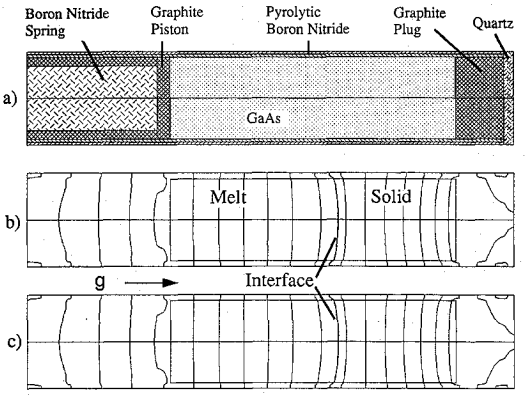

Fig. 3 a) Modeled portion of the ampule, b) isotherms at 10^{-5} gau, and c) isotherms at 1 gau, T_{min} = 1466, T_{max} = 1563°C.

residual error norms. Spatial convergence was ascertained by comparing results obtained with different grid resolutions. Typical simulations under low-gravity conditions involved approximately 7000 nodes using 4 or 9, and 8 node isoparametric elements for two-dimensional and three-dimensional computations, respectively. Two-dimensional calculations were performed with very high resolution in order to validate solution convergence. The thermophysical properties of the various materials are listed in Table 1.

Results

Results are presented for both restricted (two-dimensional) and unrestricted (three-dimensional) classes of simulations. The experimental apparatus and boundary conditions remain identical for all cases.

Restricted Modes

This class of solutions involves the traditional axisymmetric assumption for which the only admissible solutions are independent of the angular coordinate. The word "traditional" is used here to underscore the fact that the vast majority of directional solidification simulations to date involve this assumption in the formulation stage. In the absence of angular dependency, the only orientation of the gravity vector that will provide physically significant results is parallel to the ampule's longitudinal axis. When the gravity vector is tilted with respect to that axis, the flow may be three-dimensional; thus, angular dependence must be considered.

The temperature isotherms corresponding to both 1 and 10^{-5} gau are shown in Figs. 3b and 3c. The thermal conductivity mismatch among the solid, the melt (1:2 ratio), and the ampule (of less importance in this experiment) causes the interface to become concave toward the melt. At the hot end of the ampule (left), the graphite piston results in another thermal conductivity mismatch, resulting in radially curved isotherms. Note that the temperature distribution remains unchanged in spite of the strong natural convection in the 1 gau case. This result is expected for this class of semiconductors with low Prandtl number ($Pr = 0.0514$), and the relatively low Rayleigh numbers, 164 and 0.0164 (based on the measured radial temperature gradient and the radius) for 1 and 10^{-5} gau, respectively. In agreement with previous studies of similar materials,[1] the solution for the thermal field is set almost entirely by conduction alone.

The flowfields are shown in Figs. 4a and 4b as contours of stream function. Two primary cells are present. The cell adjacent to the solid/melt interface is driven by the radial thermal gradient in such a way that the hot fluid rises along the ampule's axis and descends along the walls. A counter-rotating cell is set up by the radial gradient at the hot end. This solution represents a stable state even at 1 gau. Simulations with either a steady-state scheme or with a fully implicit transient algorithm produced the same final steady state. Again, this result is expected for the low-level driving force involved, and consequently, the correspondingly small magnitude of the convective terms in the governing equations.

Table 1 Material properties

Units	
Density	g/cm^3
Latent heat	cal/g
Solute diffusivity	cm^2/s
Specific heat	cal/g-K
Temperature	K
Thermal conductivity	cal/cm-s-K
Viscosity	g/cm-s
GaAs	
Density = 5.71	
Specific heat = 0.1	
Thermal conductivity$_m$ = 0.035	
Thermal conductivity$_s$ = 0.017	
Viscosity = 0.01713	
Latent heat = 173.7	
Diffusivity of selenium in GaAs ≈ 10^{-4}	

Graphite: Density = 1.83; Specific heat = 0.19

Thermal conductivity	
Temperature	Value
300	0.3
1300	0.14
1700	0.12

Quartz: Density = 2.2

Specific heat		Thermal conductivity	
Temperature	Value	Temperature	Value
173	0.123	273	0.0034
639	0.192	750	0.0047
861	0.298	1060	0.0066
1083	0.276	1220	0.0075
1417	0.299		

Pyrolytic boron nitride: Density = 1.9

Specific heat		Thermal conductivity		
Temperature	Value	Temperature	Axial	Radial
298	0.2	298	0.25	0.004
773	0.4	773	0.17	0.005
1273	0.47	1273	0.15	0.006

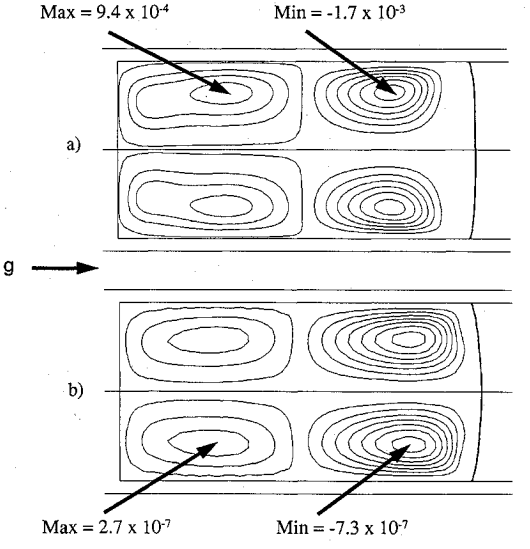

Fig. 4 Stream function at a) 1 gau and b) 10^{-5} gau.

Unrestricted Modes

In this class of solutions, the dependency of the flowfield on the azimuthal coordinate is allowed, all flow components are possible, and centerline symmetry is not invoked. An arbitrary

spatial dependency of the gravity vector is admissible for this class of solutions.

We start by presenting a duplicate study of the restricted class of solutions discussed in the previous section. When the gravity vector is aligned with the longitudinal axis, the results shown in Fig. 5 are essentially the same as those obtained using the axisymmetric model. Velocity vectors are shown (and are diluted here and in later plots for presentation) in lieu of the stream function (which is undefined in three-dimensions). It is evident that the axisymmetric mode is fully recovered, and the magnitudes of the flow velocity for both cases are identical to within a few percent of the previously computed values.

We now align the gravity vector perpendicular to the longitudinal axis. This case resembles the widely studied convection in a horizontal cylinder with imposed end temperatures. The real experimental configuration has the added complication of the coexistence of both axial and radial temperature gradients that may compete in the generation of convection patterns. Axial gradients result in a primary circulating flow rising along the hot end of the melt and descending along the cold one, similar to convection in a shallow cavity with side-wall heating. In the classical shallow cavity, such flow may be linearly unstable to both transverse or longitudinal perturbations.[8,9] The axial gradient in the melt is 6.4°C/cm. Radial gradients may result in other modes, e.g., the previously discussed axisymmetric mode, which can compete with the previous mechanism. Moreover, it is recalled that due to the complicated ampule design, the radial gradient is also a strong function of the axial position. This is illustrated in Fig. 6, in which the temperature difference between the centerline and the wall is plotted as a function of the axial position.

The selection between the modes discussed above becomes clear in Figs. 7 and 8 for the horizontal configuration. The velocity vectors on an axial slice in the x-z plane (parallel to the gravitational vector) through the centerline (Fig. 7) show the expected shallow cavity mode, with no trace of the existence of transverse secondary cells that are not expected due to geometrical considerations and the low driving Rayleigh number (3.45, based on the melt length and the axial temperature difference at 10^{-5} gau). Contours of the u (axial), the v (horizontal), and the w (vertical) velocity components are shown in Figs. 8a, 8b, and 8c, respectively, on a y-z circular cross-sectional slice at about the midsection of the melt. The contours for u show remarkable resemblance to those obtained analytically, using an asymptotic analysis by Bejan and Tien.[10] An axial velocity profile computed at a vertical slice through the centerline (Fig. 9) exhibits only slight variations

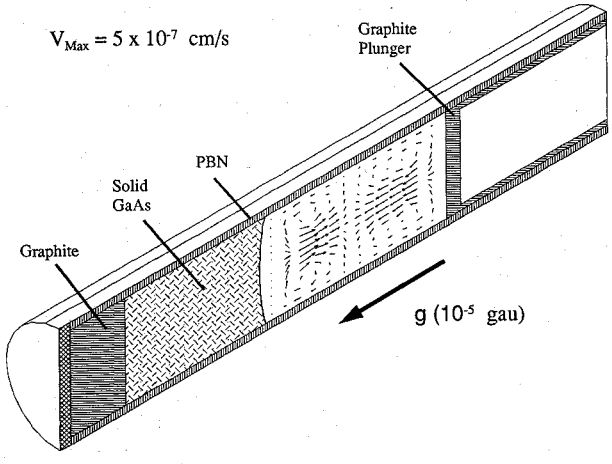

Fig. 5 Axisymmetric mode for a gravity vector aligned with the longitudinal axis.

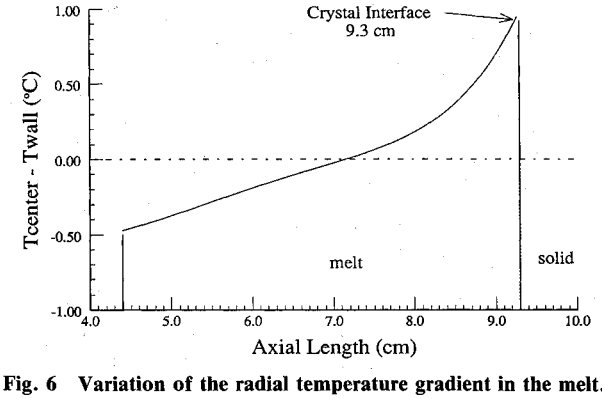

Fig. 6 Variation of the radial temperature gradient in the melt.

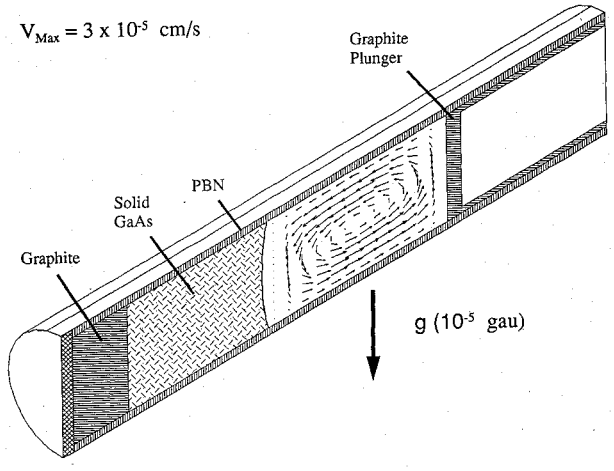

Fig. 7 Shallow cavity-type mode for a gravity vector perpendicular to the longitudinal axis.

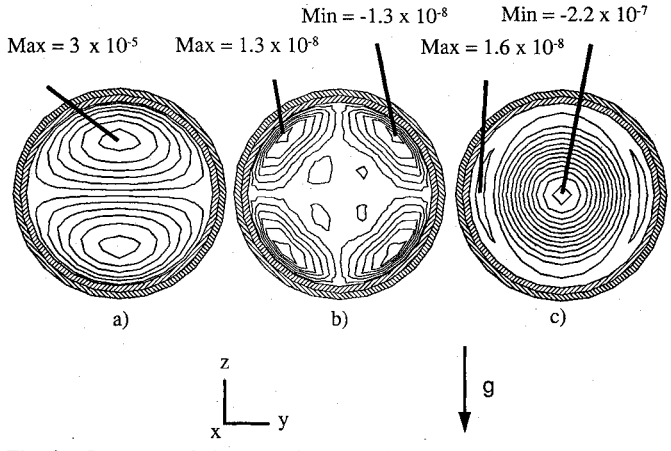

Fig. 8 Contours of a) axial, b) v, and c) w velocity components; at $x = 6.9$ cm (all velocities in cm/s).

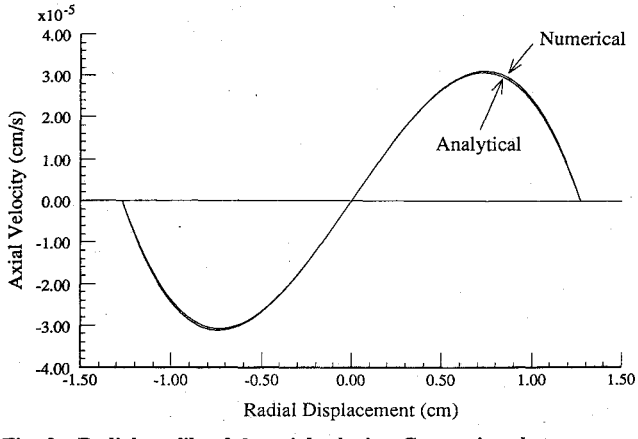

Fig. 9 Radial profile of the axial velocity. Comparison between analytical and numerical results.

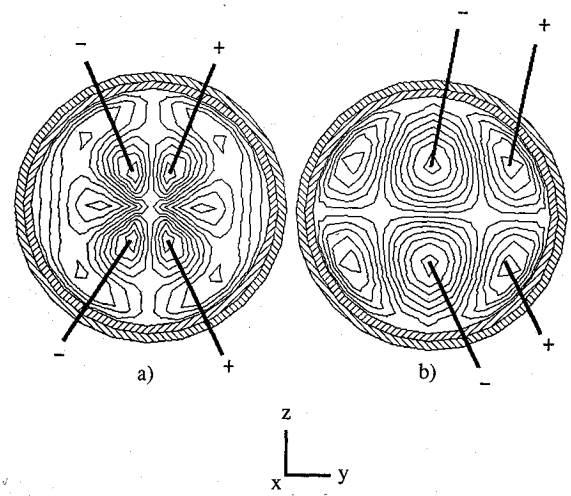

Fig. 10 Analytically predicted a) v and b) w velocity component contours.[10]

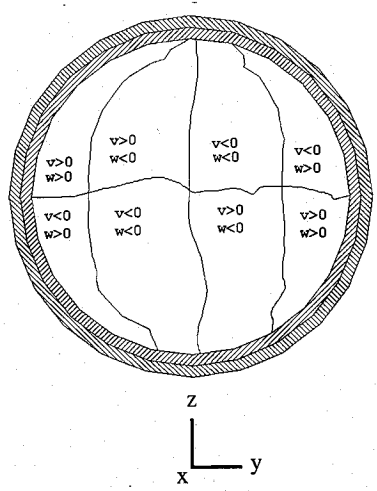

Fig. 11 Zero-crossing contours of the v and w velocities indicating two counter-rotating cells.

between the computed and predicted (to first order in the Rayleigh number) results. According to Bejan's analysis, which is based upon the conducting sidewalls assumption, the leading order (in Rayleigh number) velocities are all zero, and at first order only the axial velocity appears. At second order, the axial velocity is zero, but the other two components appear, as shown in Figs. 10a and 10b. Since the imposed radial thermal gradient is different in the GTE ampule from the idealized shallow cavity case, the secondary circulation effects are also different. Nevertheless, a zero-crossing plot[9] for the v and w velocities (Fig. 11) indicates the general feature predicted by the analysis[11] in the form of two longitudinal rolls of opposite rotation.

The general flow characteristics remain the same when the gravitational vector is placed at an intermediate angle (denoted as Θ) with respect to the ampule's axis. The magnitude of the primary axial velocity, as indicated by the maximum velocity in an x-z cross section, is proportional to the effective driving force represented by $\sin(\Theta)$ (Fig. 12). This result is expected for viscously dominated convection in space processing. For small angular displacement, the flow is dominated by the axisymmetric mode near the melt interface. A simple balance between the relative magnitudes of the operating temperature differences (axial and radial), and the effective driving forces [represented by $\sin(\Theta)$ or $\cos(\Theta)$] shows that the axisymmetric mode should dominate for angular displacements below about 0.5°C. It is also important to note that the melt velocities are much greater for the three-dimensional case (usually by two orders of magnitude).

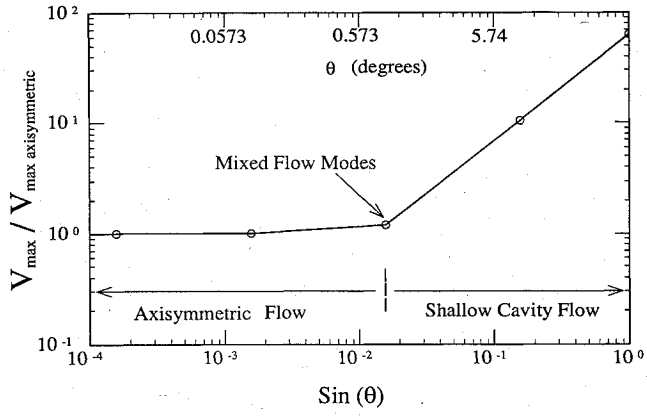

Fig. 12 Normalized velocity magnitudes vs sin(Θ).

Conclusions

The primary objective of this study was to elucidate the differences in the transport phenomena between two- and three-dimensional models for a realistic experimental apparatus. In particular, the model must be general enough to accommodate the complicated ampule geometry, end effects, and the actual furnace thermal data. Such a model represents a departure from the approach taken by other studies, in which various sets of assumptions are usually imposed. While many important and generic features of the transport phenomena in directional solidification experiments were revealed using these models, it is obvious that for many experiments, especially those designed to use advanced short aspect-ratio ampules, only models that include the entire geometrical and temporal boundary conditions information can be expected to produce realistic results.

The findings of this study naturally lead to the question of what is expected from the space processing of this or similar experiments. Although no results were presented in this study for the segregation of dopant/solutal fields, it is known that convective effects for doped semiconductor materials are important, primarily due to the low diffusivity of chemical species and consequently the high effective solutal Peclet number. For space processing, the problem of insufficient mixing of the segregation fields as elucidated by several researchers is of great practical relevance (for an excellent discussion, see Brown[1]). Results of this study suggest that utilizing axisymmetric models in predicting space experiments is not generally warranted, due to the uncertainty in the orientation of the residual gravitational acceleration vector, at least for experiments similar to the one discussed in this study. This conclusion is especially clear when one considers the extent of the presence of three- vs two-dimensional modes for arbitrary orientations, and the large increase in the flow magnitude for the three-dimensional case. A comparison among three definitions of effective solutal Peclet number, based on the radius and either the average growth rate (8.9), the maximum axisymmetric (0.006), or the maximum three-dimensional (0.38) velocities in the cell, shows that convective mixing is important for this space experiment, especially if the background gravity level increases substantially above 10^{-5} gau. The asymmetric orientation can thereby raise the susceptibility of the dopant field to convective effects by about two orders of magnitude.

It would be interesting to examine the flow and segregation fields in a classical Bridgman-Stockbarger furnace for off-axis orientation. Recent three-dimensional work by Alexander et al.[2,12] did not suggest significant variations in radial segregation from the axisymmetric mode. Additional studies envisioned include the computation of the segregation fields for the GTE experiment. Since it is evident that low-aspect ratio ampules (coupled with advanced multizone furnaces) represent a potential route to better control of the thermal environment, the conclusions of this study are of relevance to their space processing as well.

Acknowledgments

This work is sponsored by the Microgravity Science and Application Program of NASA. Useful suggestions and algorithms were obtained from Jonathan Dantzig of the University of Illinois and the staff of Fluid Dynamics International. We would also like to thank the efforts of the GTE team, including Dave Matthiesen, Brian Ditchek, Alfred Bellows, and James Kafalas. Finally, we thank Scott Coffman for his efforts in preparing the manuscript, and Emily Nelson and Tom Glasgow, who kindly reviewed it.

References

[1]Brown, R. A., "Theory of Transport Processes in Single Crystal Growth from the Melt," *AICHE Journal*, Vol. 34, No. 6, 1988, pp. 881-911.

[2]Alexander, J. I. D., Quazzani, J., and Rosenberger, F., "Analysis of the Low-Gravity Tolerance of Bridgman Stockbarger Crystal Growth—I. Steady and Impulse Accelerations," *Journal of Crystal Growth*, Vol. 97, 1989, pp. 285-302.

[3]Kafalas, J. A., and Bellows, A. H., "A Comparative Study of the Influence of Buoyancy Driven Fluid Flow on GaAs Crystal Growth," *Proceedings of the 6th European Symposium on Materials Sciences Under Microgravity Conditions*, Bordeaux, France, ESA SP-256, Feb. 1987.

[4]Engelman, M., *FIDAP Theoretical Manual*, Fluid Dynamics International, Inc., Evanston, IL, 1987.

[5]Adornato, P. M., and Brown, R. A., "The Effect of Ampule on Convection and Segregation During Vertical Bridgman Growth of Dilute and Nondilute Binary Alloys," *Journal of Crystal Growth*, Vol. 80, No. 155, 1987, pp. 155-190.

[6]Lewis, R. W., and Roberts, P. M., "Finite Element Simulation of Solidification Problems," *Applied Scientific Research*, Vol. 44, 1987, p. 61.

[7]Dantzig, J. A., "Computer Modeling of Solidification Processes," *Proceedings of CRAY Scientific & Engineering Symposium*, 1989.

[8]Kuo, H. P., Korpela, S. A., Chait, A., and Marcus, P. S., "Stability of Natural Convection in a Shallow Cavity," *Proceedings of International Heat Transfer Conf.*, 1986.

[9]Hart, J. E., "A Note on the Stability of Low-Prandtl-Number Hadley Circulations," *Journal of Fluid Mechanics*, Vol. 132, 1983, pp. 271-281.

[10]Bejan, A., and Tien, C. L., "Fully Developed Natural Counterflow in a Long Horizontal Pipe with Different End Temperatures," *International Journal of Heat & Mass Transfer*, Vol. 21, 1978, pp. 701-708.

[11]Duh, J. C., "Numerical Modeling of Enclosure Convection," *Proceedings of 40th Congress of the International Astronautical Federation*, 1989.

[12]Alexander, J. I. D., private communication, 1989.

Paul F. Mizera
Associate Editor